EFFICIENT DECONVOLUTION AND SPATIAL RESOLUTION ENHANCEMENT FROM CONTINUOUS AND OVERSAMPLED OBSERVATIONS IN MICROWAVE IMAGERY

Igor Yanovsky[1,2], *Alan Tanner*[1], *Bjorn Lambrigtsen*[1]

[1]Jet Propulsion Laboratory, California Institute of Technology, Pasadena, CA 91109
[2]University of California, Los Angeles, Joint Institute for Regional Earth System Science and Engineering, Los Angeles, CA 90095

ABSTRACT

In this paper, we develop efficient deconvolution and super-resolution methodologies and apply these techniques to reduce image blurring and distortion inherent in an aperture synthesis system. Such a system produces ringing at sharp edges and other transitions in the observed field. The conventional approach to suppressing sidelobes is to apply linear apodization, which has the undesirable side effect of degrading spatial resolution. We have developed an efficient total variation minimization technique based on Split Bregman deconvolution that reduces image ringing while sharpening the image and preserving information content. Furthermore, a proposed multiframe super-resolution method is presented that is robust to image noise and noise in the point spread function and leads to additional improvements in spatial resolution. Our super-resolution methodologies are based on current research in sparse optimization and compressed sensing, which lead to unprecedented efficiencies for solving image reconstruction problems.

Index Terms— Super-resolution, spatial resolution, sparse optimization, microwave imaging, inverse problems

1. INTRODUCTION

Hurricanes and other physically deforming phenomena will soon be continuously imaged using geostationary microwave sensors, which are designed to penetrate through thick clouds to see the structure of a storm. Such images may represent distribution of temperature, water vapor, and cloud liquid water and are valuable for evaluating the storms internal processes and its strength. The Geostationary Synthetic Thinned Aperture Radiometer (GeoSTAR) is a microwave spectrometer aperture synthesis system that has been under development at JPL since 1998 [1] and will be used to capture hurricane imagery. The instrument concept consists of an array of individual microwave receivers arranged in a Y-pattern in a plane facing the Earth. Each receiver has a small feed-horn antenna, which views the entire Earth disc, and the received signal is processed on-board to determine the cross-correlation between pairs of receivers. The cross-correlations, called visibilities, are equivalent to coefficients of a complex 2-dimensional Fourier series that represents the radiometric image of the Earth disc. The visibilities are measured between all receiver pairs simultaneously and accumulated on-board for a period of a few seconds before being downlinked to the ground for further processing. There, the visibility images are converted to radiometric images, essentially through an inverse Fourier transform (cf. Fig. 1).

A characteristic of an aperture synthesis system is that the point spread function (PSF) is a 2-dimensional sinc-like function, showing positive and negative excursions (cf. Fig. 2), that produces ringing at sharp edges and other transitions in the observed field. The conventional approach to suppressing sidelobes is to apply linear apodization, which has the undesirable side effect of degrading spatial resolution. In contrast to apodization, our approach reduces image ringing while sharpening the image and preserving information content.

Since the convolution problem in the presence of noise is highly ill-posed, regularization should be applied to achieve stability while preserving a priori properties of the solution. We formulate the restoration problem within the variational framework, using the total variation regularization. Total variation (TV) of an image measures the sum of the absolute values of its gradient and increases in the presence of the ringing artifact caused by sidelobes. By minimizing the TV of an image using the numerical techniques detailed below, our process reduces not only the ringing within the image, but is shown below to significantly reduce the brightness temperature errors in the overall image. To render these processes efficiently, our methodologies are based on current research in sparse optimization and compressed sensing. We perform the total variation based deconvolution within the Split Bregman optimization framework to achieve a factor of five hundred computational time improvement over already robust total-variation gradient descent based techniques. Additionally, a proposed multiframe super-resolution method is presented that is robust to image noise and noise in the point spread function and leads to additional improvements in spatial resolution.

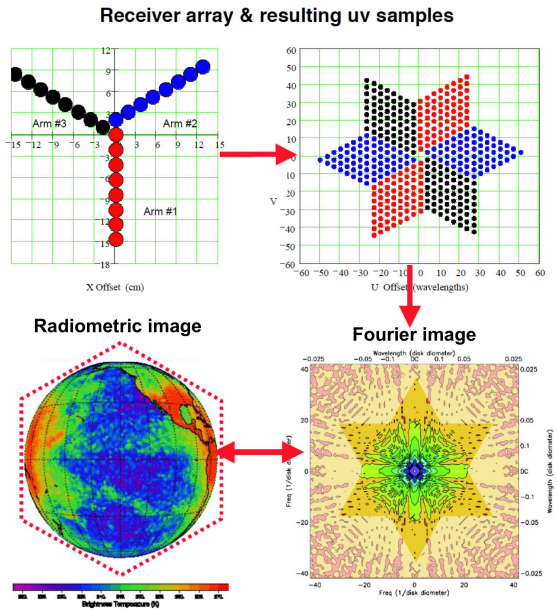

Fig. 1. Sparse array (upper left) and u-v sampling pattern (upper right), as implemented in the GeoSTAR prototype. Typical visibility magnitudes in the uv-plane (lower-right) correspond to the radiometric image (lower-left).

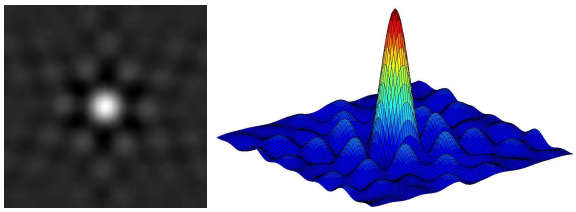

Fig. 2. The GeoSTAR point spread function.

2. NOTATION

For an image $u \in \mathbb{R}^{n\times n}$, the value of u at a pixel (i,j), with $0 \le i,j \le n$, is denoted as u_{ij}. The norms are defined as:

$$||u||_1 = \sum_{(i,j)\in\Omega} |u_{ij}|, \qquad ||u||_2 = \sqrt{\sum_{(i,j)\in\Omega} |u_{ij}|^2}.$$

The discrete gradient of u at pixel (i,j) is denoted as ∇u_{ij}, with $\nabla u_{ij} \in \mathbb{R}^2$. For a vector-valued quantity $\mathbf{d}_{ij} = ((d_1)_{ij}, (d_2)_{ij}) \in \mathbb{R}^2$, for example $\mathbf{d} = \nabla u$, the norms are defined as

$$||\mathbf{d}||_1 = \sum_{(i,j)\in\Omega} ||\mathbf{d}_{ij}||_2, \qquad ||\mathbf{d}||_2 = \sqrt{\sum_{(i,j)\in\Omega} ||\mathbf{d}_{ij}||_2^2},$$

where $||\mathbf{d}_{ij}||_2 = \sqrt{(d_1)_{ij}^2 + (d_2)_{ij}^2}$. Unless specified otherwise, $||\cdot|| = ||\cdot||_2$ in the remainder of the paper.

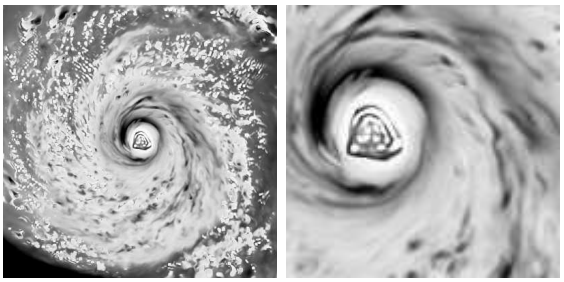

Fig. 3. Original simulated 150GHz microwave 400x400 image and its zoomed in region are shown.

3. FAST SPLIT BREGMAN DECONVOLUTION

Deconvolution process reverses effects of a blurring sensor point spread function (PSF) on observed data in the presence of noise. It is also an important step in multiframe super-resolution.

Let $u_0 \in \mathbb{R}^{n\times n}$ be an original unknown image, K be a convolution operator that represents point spread function, and $\kappa \in \mathbb{R}^{n\times n}$ be additive noise. A blurred, distorted, and noisy observation f satisfies the model

$$f = K * u_0 + \kappa. \tag{1}$$

Since the problem (1) is highly ill-posed, regularization should be applied to achieve stability while preserving a priori properties of the solution. We formulate the restoration problem within the variational framework, using the total variation regularization. Given a single observation f, we solve the deconvolution problem as TV-L_2 energy minimization

$$\min_u \ ||u||_{TV} + \frac{\mu}{2}||K*u - f||_2^2, \tag{2}$$

where u is a reconstruction and $\mu > 0$ is a weight on the L_2 norm of the residual of (1). The value of μ can be calculated automatically via Bregman iteration [2, 3]. The L_1-regularized type norm $||u||_{TV}$ measures the total variation (TV) of a signal, and is defined as $||u||_{TV} = \int |\nabla u|$, where ∇u is the gradient of u. The TV norm was originally proposed for image denoising and deblurring [4, 5] and had since been used to solve a variety of image reconstruction problems. The effectiveness of the TV norm stems from its ability to preserve edges in an image.

In [6], the authors proposed the alternating minimization algorithm for solving TV-L^2 deconvolution problems. Also, the Split Bregman algorithm for denoising images was proposed in [7]. In their paper, the authors show that the Bregman iteration can be used to solve rapidly and accurately a wide variety of constrained optimization problems. These formulations are related to problems that arise frequently in compressed sensing, where function u is reconstructed from a small subset of its Fourier coefficients [8, 9]. Inspired by

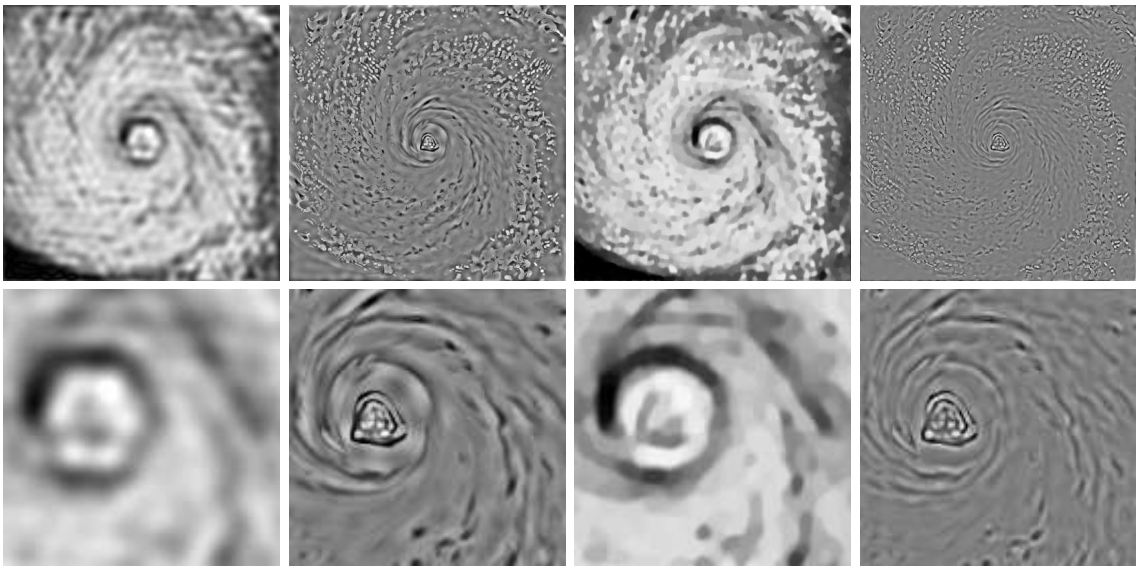

(a) Blurry and noisy 150GHz image

(b) Original Error. RMS error = 20.5 Kelvin

(c) Reconstruction

(d) Final Error. RMS error = 14.8 Kelvin

Fig. 4. Split Bregman deconvolution of a simulated 150 GHz hurricane image. (a) Original image from Figure 3 is convolved with GeoSTAR kernel from Figure 2. (b) Error between clean image and blurry image. (c) Deconvolution result. (d) Error between clean image and deconvolution result.

these methodologies, we minimize the deconvolution problem (2) within the Split Bregman minimization framework.

In order to minimize (2), an additional variable $\mathbf{d}$ is introduced to transfer ∇u out of non-differentiable terms at each pixel, and $||\mathbf{d}-\nabla u||^2$ is penalized. Hence, the Split Bregman formulation of the problem (2) is

$$\min_{u,\mathbf{d}} \quad ||\mathbf{d}||_1 \,+\, \frac{\lambda}{2}||\mathbf{d}-\nabla u-\mathbf{b}||^2 \,+\, \frac{\mu}{2}||K*u-f||^2. \quad (3)$$

Here, λ is a nonnegative parameter, and variable $\mathbf{b}$ is chosen through Bregman iteration [2, 3]: $\mathbf{b} \leftarrow \mathbf{b}+(\nabla u-\mathbf{d})$. For a fixed u, the minimization problems for $\mathbf{d}$ is

$$\mathbf{d}^* = \arg\min_{\mathbf{d}} \left\{ \,||\mathbf{d}||_1 \,+\, \frac{\lambda}{2}||\mathbf{d}-\nabla u-\mathbf{b}||^2 \,\right\},$$

which can be explicitly solved for $\mathbf{d}$, at each pixel, by using a generalized shrinkage formula [10, 11]:

$$\mathbf{d} \;=\; \max\left\{||\nabla u+\mathbf{b}||-\frac{1}{\lambda},0\right\}\frac{\nabla u+\mathbf{b}}{||\nabla u+\mathbf{b}||}.$$

For a fixed $\mathbf{d}$, the minimization problem (3) is quadratic in u:

$$u^* \;=\; \arg\min_{u} \left\{ \,||\mathbf{d}-\nabla u-\mathbf{b}||^2 \,+\, \frac{\mu}{\lambda}||K*u-f||^2 \right\},$$

and has the optimality condition:

$$\mu\tilde{K}*K*u-\lambda\triangle u = \mu\tilde{K}*f-\lambda\nabla\cdot(\mathbf{d}-\mathbf{b}), \quad (4)$$

where $\tilde{K}(x) = K(-x)$. We solve (4) using the fast Fourier transform.

We tested the method on the AMSU-B 150, 157, 166, 176, and 180 GHz channel images of hurricane Rita, shown on Figures 3 and 6. The images are 400 by 400 and were derived from the cloud resolving numerical weather prediction model (WRF) [12] simulation. We used 101 by 101 GeoSTAR point spread function K, shown on Figure 2 to blur the images.

Figure 4(a) shows 150 GHz image of Figure 3 degraded with the GeoSTAR blur. The result in Figure 4(c) is obtained using the efficient Split Bregman deconvolution model. Figures 4(b,d) show the original error and error after reconstruction as well as give root mean square (RMS) error values. In Figures 4(a,b) we see how the GeoSTAR PSF renders an image which tends to "ring" spatially to produce an unnatural appearance. In Figure 4(c), the proposed technique has produced an image which not only appears to match the true image, but in Figure 4(d) truly reduces image errors compared to Figure 4(b). Such error reductions are not realized by apodization (see Figure 5), which in fact raises the errors relative to Figure 4(b) [13]. Figure 7 shows results for other channels.

We also assessed computational efficiency of the fast fourier transform-based Split Bregman deconvolution method. Alternatively, a standard way of minimizing energy functional (2) is to use the gradient descent method. We found that solving deconvolution problem using the fast Split Bregman method is over five hundred times faster than using the gradient descent method.

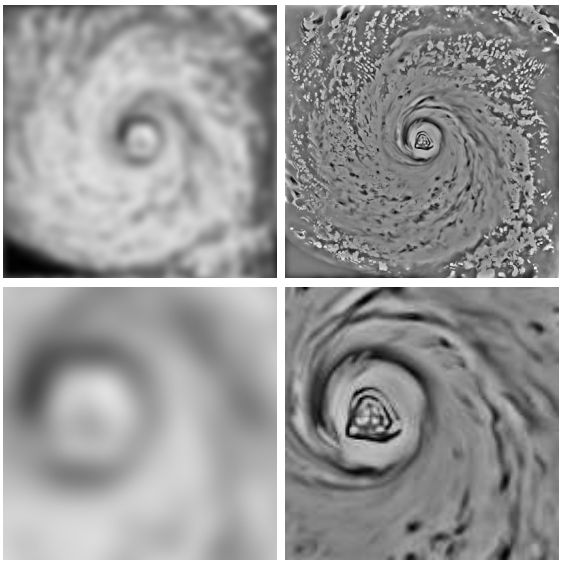

(a) Apodization result (b) Errror. RMSE = 23.5 K

Fig. 5. (a) Result obtained using conventional linear apodization method and (b) corresponding error are shown.

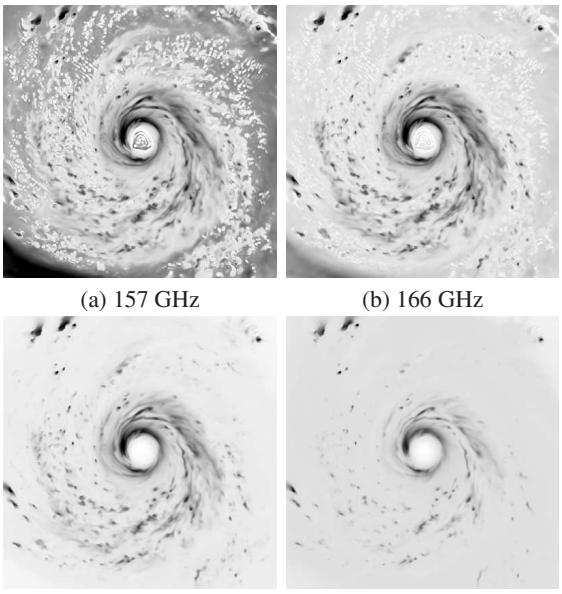

(a) 157 GHz (b) 166 GHz

(c) 176 GHz (d) 180 GHz

Fig. 6. Four microwave channels of a simulated AMSU-B multispectral 400x400 hurricane image. 150GHz channel is shown on Figure 3.

4. MULTIFRAME SUPER-RESOLUTION

Multiframe super-resolution reconstruction produces a high-resolution image from a sequence of blurry and noisy low-resolution images. We assume we are given Q noisy and blurry observations f_k, where $k = 1, \ldots, Q$. If the point spread function K contains noise s_k, the convolution model describing the relation between the unknown image u_0 and each of the observations f_k can be expressed as

$$f_k = (K + s_k) * u_0 + n_k,$$

where n_k is image noise. The PSF noise s_k may be due to contribution from the time-varying thermal misalignment and constant alignment errors, among other error sources.

Availability of oversampled observations provides for data redundancy and can be used to decrease the effects of image noise and a noisy point spread function. The minimization problem for multiframe super-resolution we consider is

$$\min_u \ ||u||_{TV} + \mu \sum_{k=1}^{Q} \omega_k ||K * u - f_k||_2^2, \qquad (5)$$

where we choose weighting constants ω_k using total variation (TV) averaging: [14]: $\omega_k = ||f_k||_{TV} / \sum_q ||f_q||_{TV}$, with $\sum_q \omega_q = 1$. The similarity term in (5) does not involve $s_k * u$ term; however, the averaging process reduces the effective noise in a point spread function, as was shown in [15]. We can re-write the minimization problem (5) as

$$\min_u \ ||u||_{TV} + \mu ||K * u - \bar{f}||_2^2, \qquad (6)$$

where $\bar{f} = \sum_k \omega_k f_k$ is weighted TV mean of the observations f_k. The signal-to-noise ratio for an average image $\bar{f}$ will be larger than that for each f_k. In [14], the authors rigorously analyzed the advantages of using multiple degraded images for reconstruction. It was shown that while high spatial frequencies of f_k are contaminated by noise, the averaging process, such as TV averaging, reduces the amplitude of high frequencies in $\bar{f}$. Hence, the minimization problem (6) allows us to recover a wider range of frequencies of u_0 as the number of images increases. We apply fast Split Bregman deconvolution to (6) as was described in the previous section.

Figures 8 and 9 show multiframe super-resolution results. Figure 8(a,b) shows noisy GeoSTAR PSF corrupted with 10% visibility error. Clean image is consecutively blurred with noisy PSF of this characteristic and is also corrupted with additive image noise of variance $\sigma^2 = 5K$ to produce a multiframe image sequence. One of the corrupted images in a sequence is displayed on Figure 8(c). Super-resolution reconstruction results are shown on Figure 9 for 3, 5, 10, and 20 frames. The quality of the reconstruction increases with the number of images in a sequence.

5. ACKNOWLEDGEMENTS

The research was carried out at the Jet Propulsion Laboratory, California Institute of Technology, under a contract with the National Aeronautics and Space Administration. The work was largely supported by NASA Weather Research program. IY also acknowledges support from the National Science Foundation Grant DMS 1217239. The authors would like to thank Svetla Hristova-Veleva, Miyoun Jung, Boon

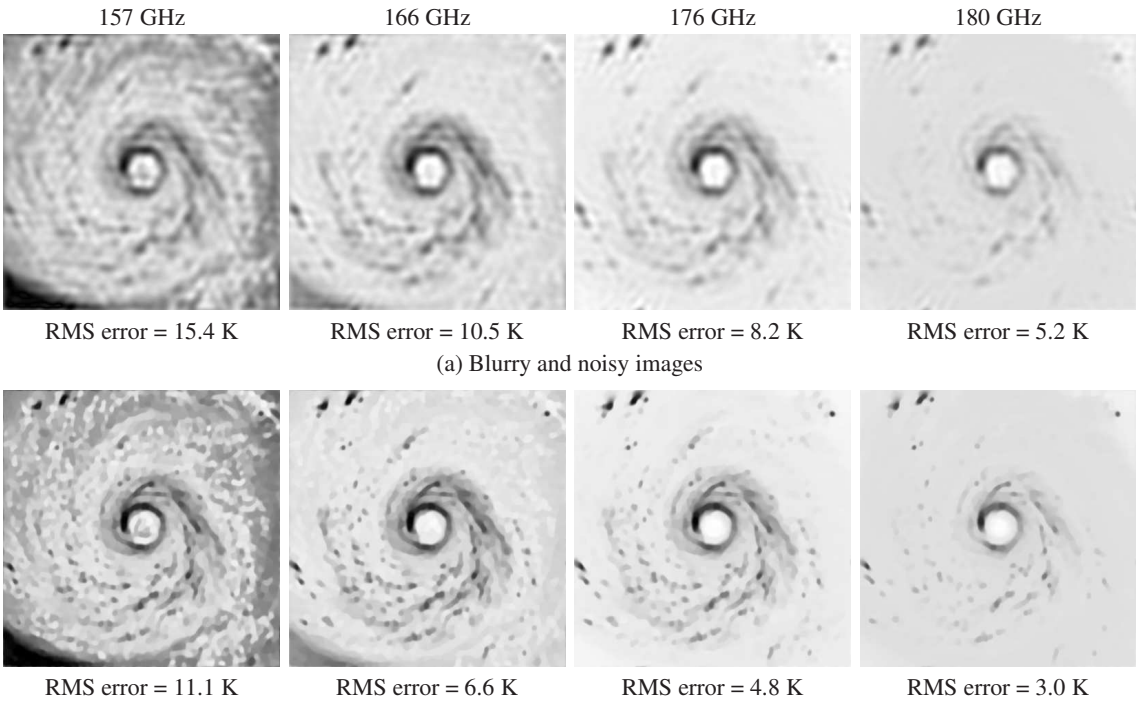

Fig. 7. Split Bregman deconvolution of simulated hurricane images. The four columns represent different microwave channels. (a) Original images from Figure 6 are convolved with GeoSTAR kernel from Figure 2. (b) Deconvolution results. Results for 150GHz channel are shown on Figure 4.

Lim, Antonio Marquina, and Luminita Vese for their helpful discussions and comments.

6. REFERENCES

[1] A.B. Tanner, W.J. Wilson, B.H. Lambrigsten, S.J. Dinardo, S.T. Brown, P.P. Kangaslahti, T.C. Gaier, C.S. Ruf, S.M. Gross, B.H. Lim, S.B. Musko, S. Rogacki, and J.R. Piepmeier, "Initial results of the Geostationary Synthetic Thinned Array Radiometer (GeoSTAR) demonstrator instrument," *IEEE Transactions on Geoscience and Remote Sensing*, vol. 45, no. 7, pp. 1947–1957, 2007.

[2] W. Yin, S. Osher, D. Goldfarb, and J. Darbon, "Bregman iterative algorithms for L1-minimization with applications to compressed sensing," *SIAM J. Imaging Sci.*, vol. 1, no. 1, pp. 143–168, 2008.

[3] S. Osher, M. Burger, D. Goldfarb, J. Xu, and W. Yin, "An iterative regularization method for total variation-based image restoration," *Multiscale Modeling & Simulation*, vol. 4, no. 2, pp. 460–489, 2005.

[4] L. Rudin, S. Osher, and E. Fatemi, "Nonlinear total variation based noise removal algorithms," *Physica D*, vol. 60, pp. 259–268, 1992.

[5] L. Rudin and S. Osher, "Total variation based image restoration with free local constraints," *IEEE International Conference on Image Processing*, vol. 1, pp. 31–35, 1994.

[6] Y. Wang, J. Yang, W. Yin, and Y. Zhang, "A new alternating minimization algorithm for total variation image reconstruction," *SIAM J. Imaging Sci.*, vol. 1, no. 3, pp. 248–272, 2008.

[7] T. Goldstein and S. Osher, "The split bregman method for L1-regularized problems," *SIAM J. Imaging Sci.*, vol. 2, no. 2, pp. 323–343, 2009.

[8] E. Candes, J. Romberg, and T. Tao, "Robust uncertainty principles: Exact signal reconstruction from highly incomplete frequency information," *IEEE Transactions on Information Theory*, vol. 52, no. 2, pp. 489–509, 2006.

[9] D. Donoho, "Compressed sensing," *IEEE Transactions on Information Theory*, vol. 52, no. 4, pp. 1289–1306, 2006.

[10] David L. Donoho and Iain M. Johnstone, "Adapting to unknown smoothness via wavelet shrinkage," *Journal of The American Statistical Association*, vol. 90, no. 432, pp. 1200–1224, 1995.

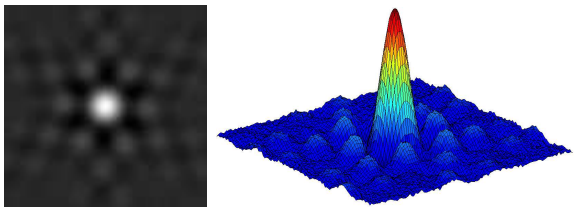

(a) Noisy GeoSTAR PSF

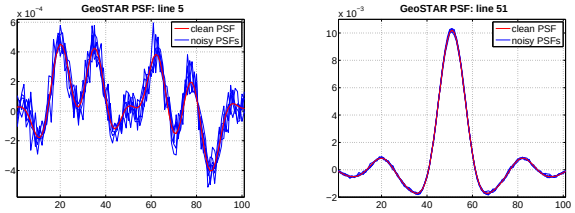

(b) Cross-sections of noisy and clean GeoSTAR PSFs

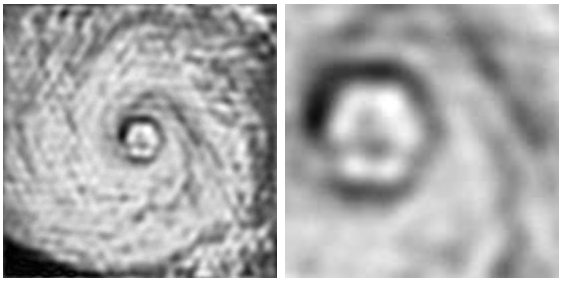

(c) Image blurred with noisy PSF from (a)

Fig. 8. (a) Noisy GeoSTAR PSF corrupted with 10% visibility error. (b) Two cross-sections of five noisy PSFs are compared with those of clean PSF. (c) Original simulated 150GHz image is blurred with noisy PSF from (a) and is further corrupted with additive image noise of variance $\sigma^2 = 5K$.

[11] Yilun Wang, Wotao Yin, and Yin Zhang, "A fast algorithm for image deblurring with total variation regularization," *CAAM Technical Report*, vol. TR07-10, 2007.

[12] J. Michalakes, J. Dudhia, D. Gill, J. Klemp, and W. Skamarock, *Design of a next-generation regional weather research and forecast model: Towards Teracomputing*, World Scientific, River Edge, New Jersey, 1998.

[13] A.B. Tanner and C.T. Swift, "Calibration of a synthetic aperture radiometer," *IEEE Transactions on Geoscience and Remote Sensing*, vol. 31, no. 1, pp. 257–267, Jan 1993.

[14] A. Marquina and S. Osher, "Image super-resolution by TV-regularization and Bregman iteration," *J. Sci. Comput.*, vol. 37, pp. 367–382, 2008.

[15] M. Jung, A. Marquina, and L. Vese, "Multiframe image restoration in the presence of noisy blur kernel," *IEEE International Conference on Image Processing*, pp. 1529–1532, 2009.

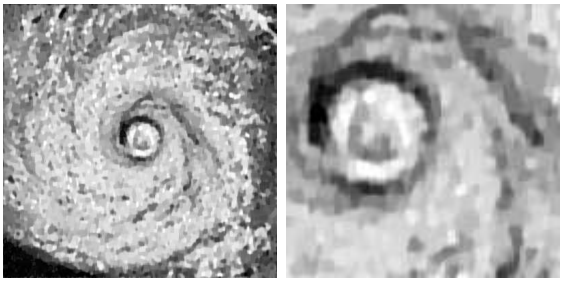

(a) 3 frames

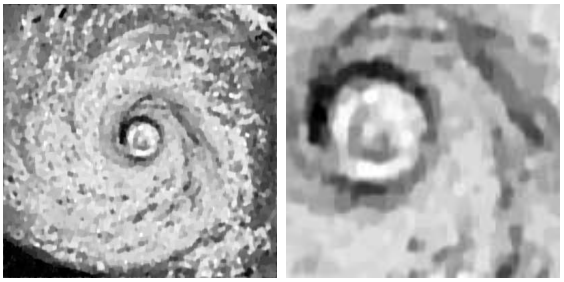

(b) 5 frames

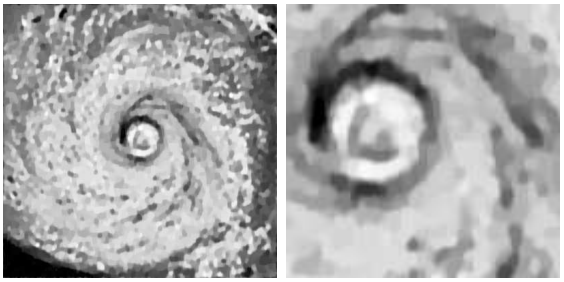

(c) 10 frames

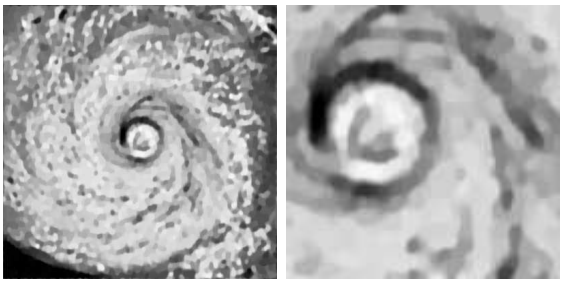

(d) 20 frames

Fig. 9. Multiframe super-resolution results. Clean image is consecutively blurred with noisy PSF (one such PSF is shown on Figure 8(a)) and is also corrupted with additive image noise of variance $\sigma^2 = 5K$ to produce an image sequence. Super-resolution reconstruction results are shown for 3, 5, 10, and 20 frames.